ELSEVIER

Suborbital-period sea-level oscillations during marine isotope substages 5a and 5c

Emma-Kate Potter [a],[*], Tezer M. Esat [a], Gerhard Schellmann [b], Ulrich Radtke [c], Kurt Lambeck [a], Malcolm T. McCulloch [a]

[a] *Research School of Earth Sciences, Australian National University, Australia*
[b] *Geographisches Institut, Universität Bamberg, Germany*
[c] *Geographisches Institut, Universität zu Köln, Germany*

Abstract

The frequency of oscillations in global ice volume as determined by dating of coral reef deposits provides an important test of the Milankovitch model of orbital climate forcing. The timing of two episodes of high sea level during marine isotope substages (MIS) 5a and 5c, here determined to have occurred at ∼ 84 and ∼ 101 ka BP are broadly consistent with the Milankovitch model. However, new high precision U-series dating of uplifted morphologically distinct coral-reef terraces at Barbados indicate that MIS-5a was both longer and more complex than previously established, with an additional sea-level highstand occurring at ∼ 77 ka BP. The U-series analysis of a large number of samples for each coral reef deposit reveals a well-defined correlation between measured age and initial $\delta^{234}U$. This correlation is evident even within the uncertainty band of ± 8‰ commonly used to exclude diagenetically altered samples and allows a more precise and accurate constraint of the age of these deposits by evaluating where the trend line intersects the modern $\delta^{234}U$ value. Other proxy climate records also indicate suborbital-period variability during MIS-5a and 5c and together imply that, as for the last ice age, orbital forcing alone cannot account for the observed changes in climate.
© 2004 Elsevier B.V. All rights reserved.

Keywords: sea level; Barbados; U-series; coral; MIS 5

1. Introduction

Climate change during the late Quaternary has been dominated by periodic large-scale oscillations between glacial and interglacial conditions. Constraining the timing and magnitude of these oscillations is essential in determining the causes of climate change. The Milankovitch insolation-forcing hypothesis suggests that global ice volume and climate are dependent on orbitally driven seasonal changes in solar insolation received at high northern latitudes [1,2]. This model is able to explain gross features of global climate over broad glacial–interglacial cycles but is not able to account for rapid, suborbital climate

* Corresponding author. Present address: Institute of Isotope Geology and Mineral Resources, ETH-Zentrum, NO F51.5, Sonneggstrasse 5, Zürich CH-8092, Switzerland. Tel.: +41-1-632-7365; fax: +41-1-632-1827.

E-mail address: potter@erdw.ethz.ch (E.-K. Potter).

fluctuations, such as those observed during the last glacial period MIS-3 [3].

Evidence of past sea-level oscillations provides a direct estimate of changes in global ice volume and hence global climate. Late Pleistocene coral reefs, where they are well preserved and accessible, can be dated using high precision U–Th techniques to con-strain the timing and magnitude of sea-level oscilla-tions. At rapidly uplifting coastlines, such as at Barbados in the West Indies and Huon Peninsula in Papua New Guinea, coral reefs that formed when sea level was below the present are now exposed above present sea level [4,5]. Previous investigations of these raised coral-reef terraces have shown they
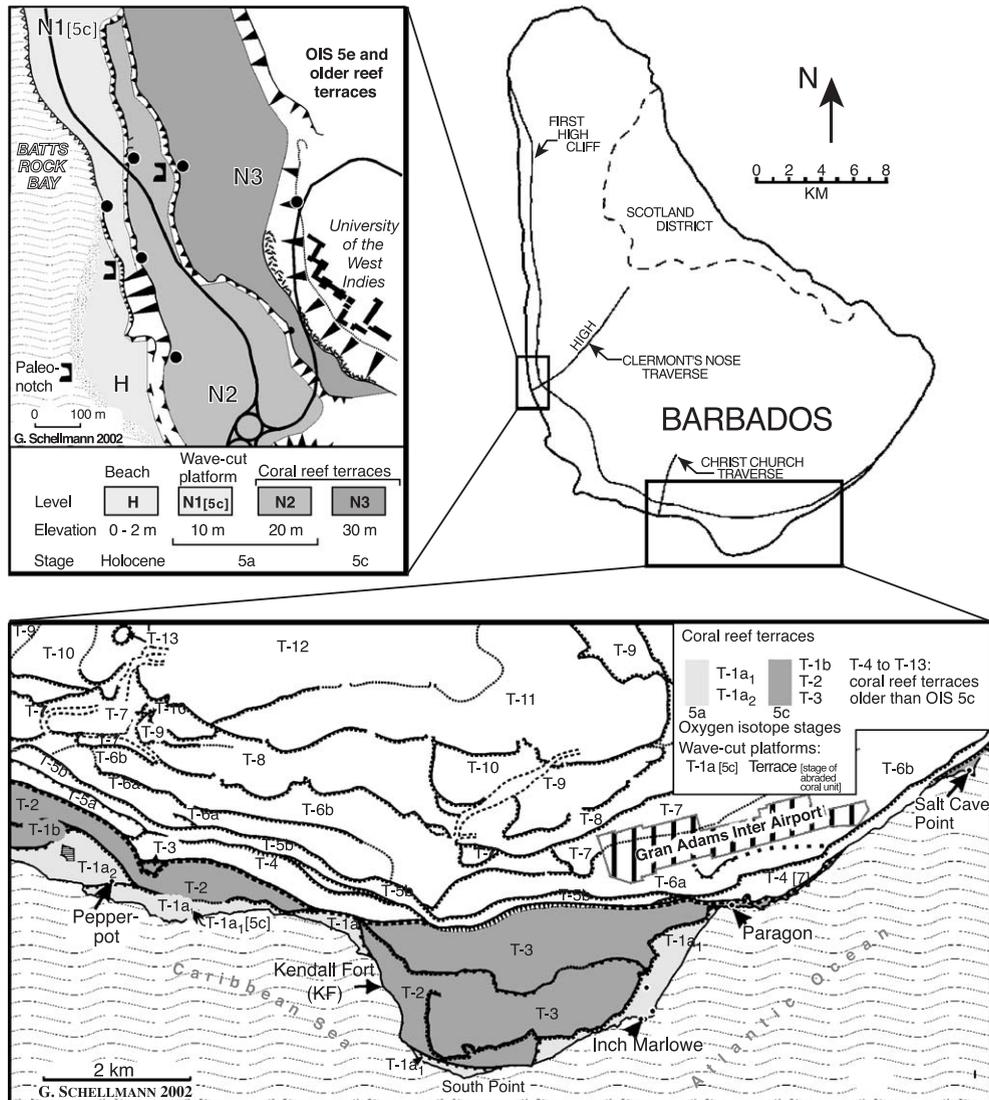

Fig. 1. The island of Barbados with MIS-5 reefs on the south and west coasts. Study sites are marked. On the south coast transect—Inch Marlowe Point (IM), Pepperpot (PEP), Kendall Fort (KF), Paragon Point (U18) and Salt Cave Point (U15). On the west coast transect—Batts Rock Bay (sites BRB1, BRB2, BRB3 and BRB4). More detailed site descriptions are given in the text. The U-series analyses for samples or sites recognised as not in situ (KF, BRB2) are included in Table 1 but not in the data summary (Fig. 2). Further details of mapping are given in [19–21].

record sea-level oscillations associated with the major glacial cycles identified in deep sea core $\delta^{18}O$ records over the last ~ 600 ka [6–8].

The end of the last interglacial (MIS-5e) was closely followed by two major interstadials, corresponding to marine isotope substages 5a and 5c. Published U-series age analyses of coral deposits suggest that the timing of these events is largely consistent with periods of high insolation. However, there is significant scatter in the age data. Previous high-precision, 'reliable' ages for the MIS-5a and 5c deposits range between ~ 76 and ~ 94 ka and ~ 100 and ~ 114 ka, respectively, at Huon Peninsula [9], Florida [10,11], Bermuda [10,12] and Barbados [13–17].

The island of Barbados is capped by coral reef terraces that formed during late Pleistocene sea-level transgressions and that have subsequently been tectonically uplifted [5]. Recently revised mapping (Fig. 1) and detailed stratigraphic study combined with ESR dating suggested that there was greater complexity in the Barbados coral terraces than previously realised [8,18–21]. Here, we present new U-series dating results of more than 70 coral samples from 9 surveyed, uplifted coral-reef deposits on the south and west coasts of Barbados. These results reveal two distinct periods of reef growth during MIS-5a, which indicates more complex variations in local sea level than expected if Milankovitch forcing was the sole cause of changes in ice volume. Based on these new observations and comparisons with other records, we address the possibility of suborbital-period sea level and climate variability within the MIS-5a and 5c interstadials.

2. Results

Samples analysed in this study were collected over two field seasons in 1999 and 2000 from surface exposures and roadcuts at Barbados. A classification of a deposit as in situ is based on observations of coral placement within the fossil reef. Unless otherwise noted, corals were sampled from at or near the crest of the terrace deposit, and therefore represent deposition during a sea-level highstand. Coral species collected include *Acropora palmata*, which generally grows within 5 m of the sea surface [22] and other coral types, such as *Monastrea* sp., *Siderastrea* sp.

and *Diploria* sp. were also collected for dating when they were clearly associated with an *A. palmata* unit and reef crest [22]. The thick walled corals such as *Diploria* sp. are generally better preserved than *A. palmata* [23].

Four in situ deposits from three distinct morphological units on the south coast, east of the standard 'Christ Church traverse', were sampled for analysis (Fig. 1). The Inch Marlowe Point sampling site (IM) is an exposed reef crest reaching up to 2 m above present sea level, predominantly consisting of shallow water (<5 m depth) *A. palmata* and other corals types associated with the back reef facies [22]. Inland of this IM deposit is a morphologically distinct reef unit, labelled 'Pepperpot' (PEP) at a maximum elevation of 4 m above present sea level. The sampling sites Paragon Point (U18) and Salt Cave Point (U15) lie eastward of the IM and PEP deposits, in a region that may have experienced a more complex uplift history according to geomorphological studies [8]. The reef crest elevation of the U18 and U15 deposits lies at 12–13 m above present sea level but an extension of that reef crest reaches 16 m above present sea level further along the coast, in the vicinity of the IM and PEP deposits [20]. The latter elevation is used for sea level calculations for those deposits. Three coral deposits judged as in situ were sampled for analysis from the west coast transect of Clermont's Nose, which has experienced the highest rate of uplift of the Barbados Coast. The lowest of the west coast sites BRB1, at Batts Rock Bay, is an exposed face reaching a maximum elevation of around 10 m above present sea level. This deposit is dominated by large head corals and no *A. palmata*, which is indicative of deep-water growth (>15 m) [22]. Site BRB3 is a reef crest deposit with a peak elevation of 19 m above present sea level. The highest Batts Rock Bay deposit, BRB4, is a reef crest at an elevation of 29 m above present sea level.

The U-series results, calculated age vs. initial $\delta^{234}U$ ($\delta^{234}U_i$), are summarised in Fig. 2. The highest elevation deposits studied here on each of the coastal transects have ages which correspond to MIS-5c. Paragon Point (U18) and Salt Cave Point (U15), have calculated ages ranging between 98 and 113 ka and initial $\delta^{234}U$ values ranging between 138‰ to 181‰. For the BRB4 deposit on the west coast, calculated
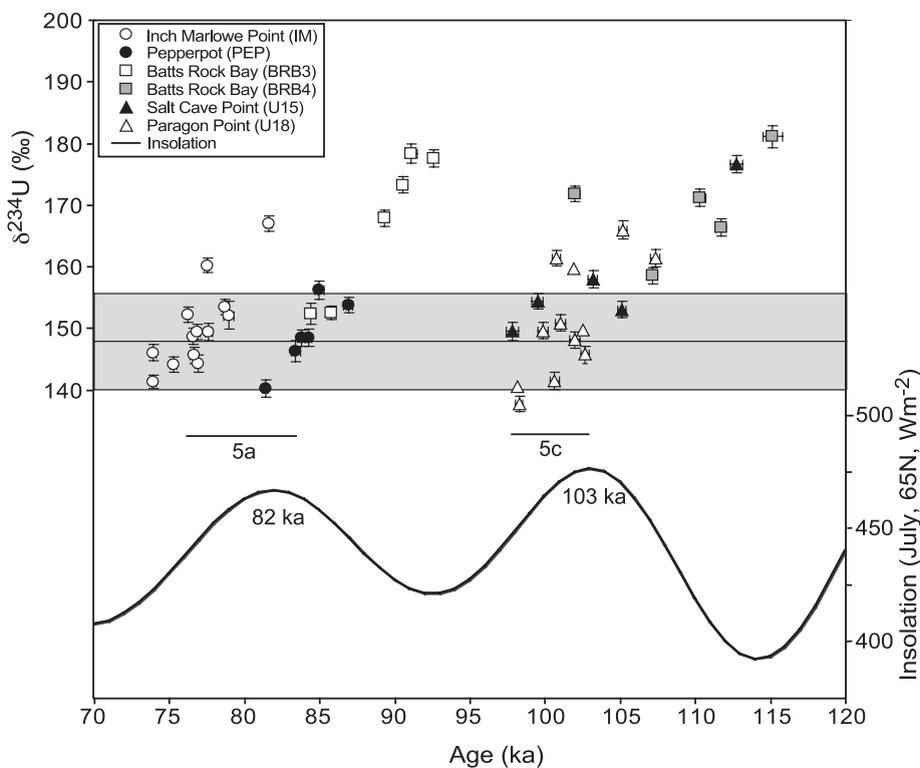
Fig. 2. Summary of U-series data for in situ, reef crest deposits (calculated age vs. $\delta^{234}U_i$) from this study and comparison with July 65°N insolation forcing curve [51]. Site BRB1, even though it is an in situ deposit, is not included here because it represents deep water growth and therefore its relationship to the timing of a sea-level highstand is not clear. The shaded region defines the generally accepted ± 8‰ band of $\delta^{234}U$ values that define a reliable age (to within 2 ka). The age and $\delta^{234}U_i$ data from each site display a rough linear correlation. A similar trend has also been described in previous studies, however in this case the trend is clearly identifiable even within the 8‰ $\delta^{234}U$ band, especially for the two younger deposits. If the oceanic $\delta^{234}U$ at the time of deposition of these corals was equal to the present-day value, the timing of each event can be accurately and precisely determined by where the trend line intersects the modern $\delta^{234}U_i$ value of 149‰. Summary of total data set, including samples not in growth position is given in Table 1. The timing of the peak sea level for the "classic" MIS-5a and 5c events at 84 and 101 ka coincide with or slightly postdate the associated insolation peak, consistent with the Milankovitch model of insolation forcing. The presence of an additional MIS-5a highstand, identified in this study at 77 ka BP, demonstrates that orbital forcing alone cannot account for the observed changes in ice volume during this period.

ages range between 102 and 122 ka ($\delta^{234}U_i = 159‰$ to 172‰). The PEP and BRB3 deposits on the south and west coasts, respectively, represent reef growth during MIS-5a. PEP corals yield ages of between 81.5 and 87 ka ($\delta^{234}U_i = 140‰$ to 156‰) and BRB3 between 85 and 93 ka ($\delta^{234}U_i = 152‰$ to 178‰). Calculated coral ages for the IM deposit on the south coast are distinct from the classic MIS-5a deposits and range between 74 and 82 ka ($\delta^{234}U_i = 141‰$ to 167‰). Details of the results are given in Table 1.

Veracity of coral U-series ages depends on the quality of coral samples and can be affected by diagenetic alteration. Criteria have been developed

to assess the reliability of U-series ages including (i) physical signs of dissolution and recrystallisation determined from petrographic examination of thin sections, (ii) degree of recrystallisation of primary aragonite to calcite observed using X-ray diffraction, (iii) uranium concentration, (iv) presence of detrital thorium contamination inferred from [232]Th concentration and (v) comparison of calculated initial $\delta^{234}U$ with that of modern corals as an indicator of uranium and thorium isotope mobilisation [15]. [231]Pa dating has also been used to evaluate the reliability of U-series ages [24]. Several recent studies have dealt with the effects of diagenetic

Table 1
Isotope ratios and U-series age measurements for samples analysed in this study

Sample number	Coral type[a]	XRD	Elevation[b] (m asl)	^{238}U (ppm)	^{232}Th (ppb)	$\delta^{234}U_m$[c] (‰)	$^{230}Th/^{238}U$ activity	Age[d] (ka)	$\delta^{234}U_i$[e] (‰)
Inch Marlowe Point									
IM1-1	S	<1%	1.5	2.20	0.23	121.5 ± 1.9	0.5861 ± 0.0013	79.1 ± 0.3	152.0 ± 2.3
IM1-2	S	<1%	1.5	2.29	0.28	122.7 ± 1.1	0.5852 ± 0.0008	78.8 ± 0.2	153.4 ± 1.3
IM1-3a	S	–	1.5	2.19	0.18	119.6 ± 1.1	0.5726 ± 0.0007	76.7 ± 0.2	148.7 ± 1.3
IM1-4	S	<1%	1.5	2.02	0.04	122.6 ± 1.0	0.5725 ± 0.0006	76.3 ± 0.2	152.2 ± 1.2
IM1-5	S	<1%	1.5	2.17	0.31	120.1 ± 1.1	0.5742 ± 0.0008	76.9 ± 0.2	149.3 ± 1.3
IM1-6	S	<2%	1.5	2.26	0.26	118.3 ± 1.1	0.5581 ± 0.0007	74.1 ± 0.2	146.0 ± 1.3
IM1-7	S	<1%	1.5	2.19	0.18	128.5 ± 1.0	0.5825 ± 0.0007	77.6 ± 0.2	160.2 ± 1.2
IM1-8	Ap	–	1.5	2.81	0.02	114.5 ± 1.0	0.5560 ± 0.0008	74.0 ± 0.2	141.3 ± 1.1
IM1-10	S	<1%	2	1.99	0.15	115.9 ± 1.2	0.5723 ± 0.0007	77.0 ± 0.2	144.2 ± 1.4
IM1-11	Ap	–	1.5	3.47	0.06	132.5 ± 1.0	0.6060 ± 0.0008	81.7 ± 0.2	167.0 ± 1.2
IM1-12	Ap	–	0.2	2.92	0.03	117.1 ± 1.1	0.5715 ± 0.0012	76.7 ± 0.3	145.6 ± 1.3
IM1-13	Ap	<1%	0.2	2.97	0.04	116.4 ± 1.0	0.5640 ± 0.0009	75.4 ± 0.2	144.1 ± 1.2
IM1-14	Ap	<1%	0.2	3.14	0.04	119.8 ± 1.1	0.5783 ± 0.0012	77.7 ± 0.3	149.4 ± 1.3
Pepperpot									
PEP1-1	S	–	2.5	2.22	0.04	111.2 ± 1.1	0.5924 ± 0.0006	81.5 ± 0.2	140.1 ± 1.4
PEP1-2	Ap	–	2.5	3.17	0.08	122.7 ± 1.2	0.6169 ± 0.0013	85.1 ± 0.3	156.1 ± 1.4
PEP1-3	Ap	<1%	2.5	2.46	0.03	117.0 ± 1.1	0.6075 ± 0.0009	83.9 ± 0.2	148.4 ± 1.3
PEP1-4	S	–	2.5	2.34	0.04	115.4 ± 1.4	0.6047 ± 0.0012	83.5 ± 0.3	146.2 ± 1.7
PEP1-5	S	–	2.5	2.35	0.06	116.9 ± 1.2	0.6101 ± 0.0007	84.4 ± 0.2	148.4 ± 1.5
PEP1-6	S	–	3	3.27	0.03	120.1 ± 1.1	0.6245 ± 0.0012	87.0 ± 0.3	153.7 ± 1.3
Salt Cave Point									
U15-2	D	–	4.2	2.44	0.22	113.7 ± 1.0	0.7311 ± 0.0012	113.2 ± 0.4	156.6 ± 1.3
U15-3	Ap	–	5.2	3.20	0.10	128.2 ± 1.1	0.7407 ± 0.0014	112.9 ± 0.4	176.6 ± 1.4
U15-4	Ap	–	5.4	3.50	0.12	113.2 ± 1.1	0.6699 ± 0.0015	97.9 ± 0.4	149.4 ± 1.4
U15-6	Ap	–	5.2	3.37	0.12	133.2 ± 1.1	0.7256 ± 0.0014	108.1 ± 0.4	180.9 ± 1.4
U15-7	Ap	–	6.7	3.56	0.12	116.4 ± 1.0	0.6793 ± 0.0013	99.6 ± 0.3	154.3 ± 1.3
U15-10	Ap	–	4	3.26	0.06	95.7 ± 1.1	0.8781 ± 0.0026	168.2 ± 2.4	154.2 ± 1.9
U15-16	Ap	–	10.3	3.10	0.11	117.8 ± 1.1	0.6961 ± 0.0011	103.3 ± 0.3	157.9 ± 1.3
U15-17	Ap	–	12.5	3.23	0.15	113.5 ± 1.1	0.7010 ± 0.0008	105.2 ± 0.3	153.0 ± 1.3
Kendall Fort									
KF-1	Ap	–	1.1	3.72	0.05	132.6 ± 1.0	0.6113 ± 0.0010	82.8 ± 0.2	167.7 ± 1.2
KF-2	Ap	–	1.6	3.20	0.06	130.5 ± 1.1	0.6481 ± 0.0013	90.6 ± 0.3	168.7 ± 1.4
KF-3	S	–	2	2.51	0.36	123.0 ± 1.3	0.6223 ± 0.0011	86.2 ± 0.3	157.0 ± 1.5
KF-3b	Ap	–	2	3.94	0.03	150.7 ± 1.2	0.6661 ± 0.0015	91.7 ± 0.4	195.4 ± 1.5
KF-4	S	–	3	2.12	0.01	122.8 ± 1.1	0.6189 ± 0.0009	85.5 ± 0.2	156.4 ± 1.3
KF-5	D	–	3.5	2.19	0.03	113.0 ± 1.8	0.6024 ± 0.0013	83.3 ± 0.3	143.2 ± 2.2
KF-6	S	–	4	2.42	0.03	117.9 ± 1.1	0.6037 ± 0.0009	83.0 ± 0.2	149.1 ± 1.3
KF-8	S	–	7	2.36	0.13	114.2 ± 1.0	0.5985 ± 0.0008	82.4 ± 0.2	144.2 ± 1.2
Paragon Point									
U18-1	Ap	<1%	1.3	3.03	0.11	113.2 ± 1.0	0.6838 ± 0.0012	101.2 ± 0.3	150.8 ± 1.3
U18-2	Ap	<1%	2.3	3.14	0.12	119.5 ± 1.0	0.6917 ± 0.0013	102.0 ± 0.4	159.6 ± 1.2
U18-3	Ap	<1%	2.8	3.06	0.11	106.3 ± 1.0	0.6667 ± 0.0013	98.3 ± 0.3	140.4 ± 1.3
U18-4	S	<1%	3.2	2.49	0.11	123.1 ± 1.2	0.7071 ± 0.0009	105.3 ± 0.3	165.9 ± 1.5
U18-5	Ap	<1%	4.3	3.43	0.14	106.3 ± 1.1	0.6772 ± 0.0011	100.7 ± 0.3	141.4 ± 1.3
U18-6	Ap	<1%	4.9	3.27	0.10	110.8 ± 1.0	0.6861 ± 0.0011	102.1 ± 0.3	148.0 ± 1.3
U18-9	Ap	<1%	4.5	2.92	0.08	104.2 ± 1.0	0.6658 ± 0.0008	98.4 ± 0.3	137.7 ± 1.3

Table 1 (*continued*)

Sample number	Coral type[a]	XRD	Elevation[b] (m asl)	^{238}U (ppm)	^{232}Th (ppb)	δ^{234}U$_m$[c] (‰)	^{230}Th/^{238}U activity	Age[d] (ka)	δ^{234}U$_i$[e] (‰)
Paragon Point									
U18-10	Ap	<2%	5.8	3.27	0.10	112.7 ± 1.0	0.6784 ± 0.0012	100.0 ± 0.3	149.6 ± 1.3
U18-13	S	<1%	4.9	2.22	0.14	119.0 ± 1.1	0.7129 ± 0.0010	107.4 ± 0.3	161.3 ± 1.4
U18-18	Ap	<1%	6.7	3.34	0.10	121.3 ± 1.0	0.6880 ± 0.0009	100.8 ± 0.3	161.4 ± 1.2
U18-19	Ap	–	9.6	2.98	0.16	111.9 ± 1.1	0.6890 ± 0.0011	102.6 ± 0.3	149.7 ± 1.3
U18-20	M	–	9.6	2.44	0.13	108.9 ± 1.0	0.6875 ± 0.0009	102.8 ± 0.3	145.7 ± 1.3
Batts Rock Bay (site 1)									
BRB1-2	S	–	2.1	2.08	0.16	113.5 ± 1.4	0.7000 ± 0.0008	105.0 ± 0.3	152.9 ± 1.7
BRB1-5	D	–	1.8	2.25	0.26	108.7 ± 1.1	0.7068 ± 0.0007	107.8 ± 0.3	147.5 ± 1.4
BRB1-6	M	<1%	3.4	2.21	0.09	109.8 ± 1.0	0.6922 ± 0.0011	103.7 ± 0.3	147.3 ± 1.3
BRB1-7	M	<2%	1.4	2.45	0.24	108.0 ± 1.1	0.7077 ± 0.0013	108.1 ± 0.4	146.7 ± 1.4
BRB1-13	S	–	2.4	2.00	0.02	114.1 ± 1.1	0.7038 ± 0.0009	106.0 ± 0.3	154.2 ± 1.4
BRB1-14	S	–	3.1	2.34	0.10	116.9 ± 1.1	0.7037 ± 0.0009	105.5 ± 0.3	157.7 ± 1.4
BRB1-15	S	<1%	3.3	2.25	0.07	113.4 ± 1.0	0.6941 ± 0.0010	103.6 ± 0.3	152.1 ± 1.3
BRB1-16	D	–	10	2.27	0.51	109.6 ± 1.2	0.6077 ± 0.0007	84.8 ± 0.2	139.3 ± 1.4
BRB1-18	M	–	8.5	2.57	0.83	107.8 ± 1.0	0.6861 ± 0.0010	102.6 ± 0.3	144.2 ± 1.3
Batts Rock Bay (site 2)									
BRB2-2	Ap	–	14.3	2.85	0.12	116.1 ± 1.1	0.5945 ± 0.0011	81.3. ± 0.3	146.2 ± 1.3
BRB2-3	S	–	14.3	1.78	0.16	119.6 ± 1.0	0.5476 ± 0.0008	72.0 ± 0.2	146.7 ± 1.2
BRB2-6	S	–	12.5	2.27	0.19	114.5 ± 1.0	0.5883 ± 0.0008	80.3 ± 0.2	143.8 ± 1.2
BRB2-7	S	–	12.5	1.97	0.04	112.9 ± 1.0	0.5803 ± 0.0008	78.9 ± 0.2	141.2 ± 1.2
Batts Rock Bay (site 3)									
BRB3-1	Ap	–	26.5	3.35	0.03	130.3 ± 1.1	0.6422 ± 0.0013	89.4 ± 0.3	167.9 ± 1.3
BRB3-2	Ap	–	16.5	2.75	0.05	119.9 ± 1.5	0.6124 ± 0.0015	84.5 ± 0.4	152.3 ± 1.8
BRB3-3	Ap	–	16.5	3.25	0.04	137.7 ± 1.3	0.6556 ± 0.0015	91.2 ± 0.4	178.4 ± 1.6
BRB3-5	Ap	–	16.5	3.24	0.03	136.5 ± 1.1	0.6617 ± 0.0013	92.7 ± 0.3	177.6 ± 1.4
BRB3-8	Ap	–	16.5	3.63	0.03	119.5 ± 0.9	0.6186 ± 0.0014	85.8 ± 0.3	152.5 ± 1.1
BRB3-9	S	–	19	2.34	0.03	134.0 ± 1.1	0.6506 ± 0.0008	90.7 ± 0.2	173.3 ± 1.3
Batts Rock Bay (site 4)									
BRB4-1	Ap	–	30	3.10	0.12	130.6 ± 1.4	0.7516 ± 0.0023	115.3 ± 0.7	181.1 ± 1.8
BRB4-4	Ap	–	29.9	3.17	0.19	113.7 ± 1.1	0.7647 ± 0.0015	122.4 ± 0.9	160.8 ± 1.5
BRB4-7	Ap	–	28.1	2.80	0.07	121.2 ± 1.1	0.7316 ± 0.0011	111.8 ± 0.4	166.4 ± 1.4
BRB4-8	S	–	28.5	2.38	0.07	116.9 ± 1.1	0.7107 ± 0.0011	107.3 ± 0.3	158.5 ± 1.3
BRB4-9	Ap	–	29.1	2.87	0.03	125.1 ± 1.1	0.7291 ± 0.0011	110.4 ± 0.3	171.1 ± 1.4
BRB4-10	Ap	–	28	3.20	0.32	128.6 ± 1.0	0.6985 ± 0.0013	102.1 ± 0.3	171.8 ± 1.3

In situ sample deposits (bolded) are Inch Marlowe Point (IM), Pepperpot (PEP), Paragon Point (U18) and Salt Cave Point (U15) on the south coast and Batts Rock Bay (sites BRB1, BRB3 and BRB4) on the west coast. Data from the Kendall Fort (KF) and Batts Rock Bay 2 (BRB2) sites are not in situ deposits and are not included in the summary (Fig. 2). [a] Coral type given as: Ap—*Acropora palmata*, S—*Siderastrea* sp., M—*Montastrea* sp., D—*Diploria* sp. XRD—% calcite of sample determined by X-ray diffraction, where measured, most samples contained less than the detection limit of 1–2%. [b] Elevation above present sea level (m), elevation uncertainty for individual coral elevations is ± 0.5 m. [c] Present-day measured δ^{234}U calculated by δ^{234}U$_m$={[^{234}U/^{238}U]$_{activity}$ − 1} × 10^3. [d] U-series age equation, see [53]. [e] Initial δ^{234}U given by δ^{234}U$_i$ = δ^{234}U$_m$e$^{\lambda 234 \times T}$. Quoted uncertainties reflect analytical precision only and do not take into account uncertainties in decay half-lives of ^{234}U or ^{230}Th. Conventional decay constants are used: λ_{238} = 1.551 × 10^{-10}, λ_{234} = 2.835 × 10^{-6}, λ_{230} = 9.195 × 10^{-6} [54–56]. Procedures for the chemical separation and purification of uranium and thorium from the coral samples were similar to those described by Edwards et al. [57] and Stirling et al. [23]. Uranium analyses were made by thermal ionisation mass spectrometry (TIMS) with a Finnigan MAT 261 and thorium analyses by charge collection thermal ionisation mass spectrometry (CC-TIMS) [58]. Isotope dilution was performed with a mixed ^{233}U–^{229}Th tracer, calibrated against Harwell Uraninite standard (HU-1), which was assumed to be in secular equilibrium [59]. All uncertainties are quoted as 2σ_M.

alteration on U-series ages [25–27] but the mechanisms are not yet completely understood. Our study confirms that there is no clear correspondence between petrographic textures and U-series results in subtly altered corals. To avoid the risk of over-interpreting isolated age measurements, we have therefore analysed a large number of samples from each study site and we believe that this strategy is as important as the other tests of age reliability.

3. U-series age interpretations

Modern corals display δ^{234}U values of ~ 149 ± 1‰ [10,14,15,28–30] (conventional ^{230}Th and ^{234}U half-lives are used throughout this paper, see Table 1). Previous coral dating studies of last interglacial (MIS-5e) and older samples show a general positive correlation of calculated age and initial δ^{234}U above the δ^{234}U modern value for a given deposit, which has been attributed to open system behaviour [15,25,31]. Based on the observed correlation, it has been suggested that samples with δ^{234}U$_i$ values within 8‰ of the modern value yield ages that are reliable to within 2–3 ka [15,25] and many researchers have adopted this screening approach (shown in Fig. 2) to allow for uncertainties introduced by subtle alteration processes [15,17].

The striking features of the data shown in Fig. 2 are, firstly, the distinct clustering of coral ages from morphologically distinct terraces into two groups within MIS-5a and secondly, the high correlation between δ^{234}U$_i$ and age within each of these groups, which is well defined even within the commonly used ± 8‰ band both below and above the modern δ^{234}U value. If the trend lines are the result of diagenetic alteration [15,25,31] and if we assume that the sea water δ^{234}U at the time of growth was the same as the present day, then the age of each feature is defined by the age at which the trend line intersects the modern δ^{234}U value. For both of the MIS-5a features, a linear regression and associated uncertainty analysis was performed in δ^{234}U$_m$ vs. [^{230}Th/^{238}U]$_{ACT}$ space (Fig. 3). The scatter of data around a given trend line could represent either (i) scatter resulting from the alteration process or (ii) a spread in the true ages of samples collected from that deposit. In the former case, we wish to determine a mean age and confidence interval for
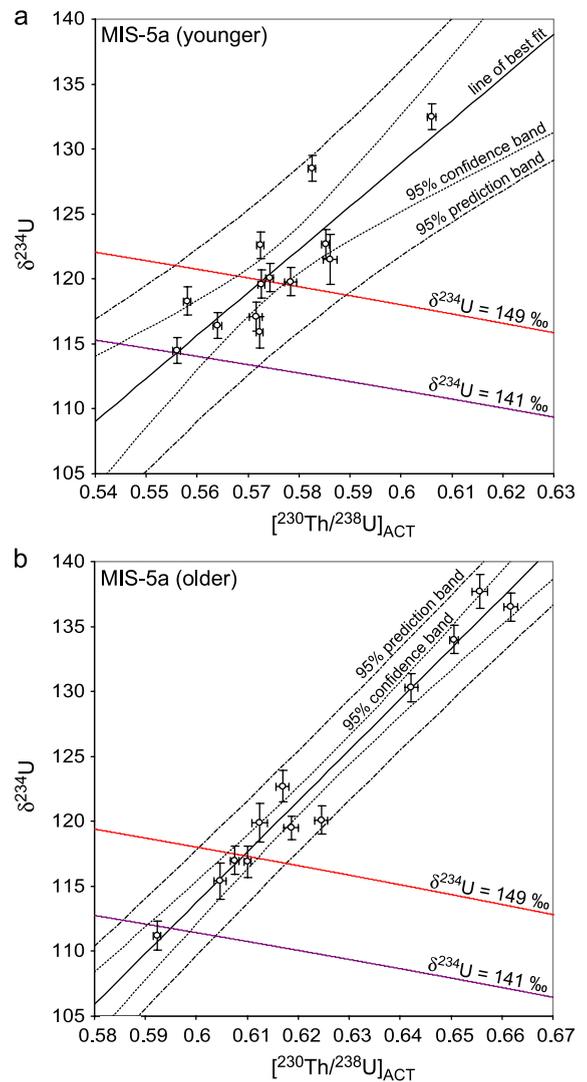

Fig. 3. Determination of line of best fit and 95% confidence and prediction bands for the younger (a) and older (b) MIS-5a features. The representative δ^{234}U$_m$ and [^{230}Th/^{238}U]$_{ACT}$ values for each feature are determined by estimating where the line of best fit intersects the evolution curve for a chosen initial δ^{234}U value. The uncertainties for the δ^{234}U$_m$ and [^{230}Th/^{238}U]$_{ACT}$ parameters for each feature are determined using either the 95% confidence band or 95% prediction band and these errors are propagated through the U-series age equation to calculate a mean age or duration of deposition, respectively. The representative δ^{234}U$_m$ and [^{230}Th/^{238}U]$_{ACT}$, and hence age estimates, for these deposits change depending on the assumed initial δ^{234}U value.

each deposit. The intersection of the 95% confidence band of the regression with the closed system evolution curve ($\delta^{234}U = 149‰$) was used to determine the 95% confidence interval associated with the representative $\delta^{234}U_m$ and $[^{230}Th/^{238}U]_{ACT}$ for that deposit. Using this procedure, two distinct periods of reef growth can be identified, with mean ages and uncertainties determined to be 76.7 ± 1.0 and 84.3 ± 0.7 ka BP. For the second case, if the scatter of the data represents a true age range, the spread of the data around the trend line, represented by a 95% prediction band of the regression, can give an estimate of the total age range. In that case, the age estimates for the younger two features are 76.7 ± 3.3 and 84.3 ± 1.8 ka. The mean U-series ages presented here agree well with ESR ages (73.4 ± 5 and 80.9 ± 5 ka) for the same deposits [21] and are consistent with detailed stratigraphic mapping, which indicate that the IM and PEP deposits are also distinct morphological units [20].

The spread of the MIS-5c data around its associated trend line is larger than for the other deposits and the scatter appears to increase at higher $\delta^{234}U$ and $[^{230}Th/^{238}U]_{ACT}$ values, making the use of a linear regression inappropriate for this feature. At the modern $\delta^{234}U$ value of 149‰, the mean age of the samples analysed is ~ 101 ka. Based on an approximation of the scatter of the data in Fig. 2, the data could represent an extended period of reef growth of at least ~ 5 ka, from ~ 103 to ~ 98 ka BP. This extended age range may also be due to the slightly larger elevation range of corals collected from these deposits on the south coast (Table 1).

Previous studies into the effects of diagenetic alteration have focussed on the mechanisms to explain the positive correlation between $\delta^{234}U$ and $[^{230}Th/^{238}U]_{ACT}$ above the modern $\delta^{234}U$ evolution curve [15,25–27]. However, a significant number of samples analysed in this study (Fig. 2 and Table 1) display $\delta^{234}U_i$ values well below the modern 149‰ value and the $\delta^{234}U$-age trend appears to start as low as $\delta^{234}U_i \approx 140‰$. Recent open system modelling suggests the loss of ^{234}Th and ^{230}Th, from decay of ^{238}U and ^{234}U, respectively, in some "source" leads to the positive correlation between $\delta^{234}U_m$ and $[^{230}Th/^{238}U]_{ACT}$ observed in the coral [25,26]. In this model, the source of the excess ^{234}U (^{234}Th) and ^{230}Th is recoil products of ^{238}U and ^{234}U in the surrounding reef or dissolved uranium in

percolating fluids [25]. By a similar mechanism, the lowering of $\delta^{234}U$ and $[^{230}Th/^{238}U]_{ACT}$ in corals could be produced by recoil loss of ^{234}Th and ^{230}Th [25] or alternatively, the addition of low $\delta^{234}U$ contamination [27]. If either process is responsible for the lower-than-modern $\delta^{234}U_i$ values of MIS-5a corals observed in this study, then we would expect such low values to be even more common in older deposits, which is not observed.

An alternative scenario to explain the low initial $\delta^{234}U$ values observed here invokes a lowering of ocean water $\delta^{234}U$ during the last glacial cycle. In this case, the age versus $\delta^{234}U$ trend would represent the effects of diagenetic alteration starting from a lower-than-modern initial $\delta^{234}U$. The observation of lower-than-modern $\delta^{234}U$ is not unprecedented. MIS 3 coral-deposits from the uplifted terraces at Huon Peninsula, Papua New Guinea, also display consistently low initial $\delta^{234}U$ values (130–145‰) [32,33]. If seawater $\delta^{234}U$ was lower-than-modern, i.e. 141‰, at the time of MIS-5a and 5c, this has critical implications for the age estimates of these features. The younger MIS-5a event then occurs at $\sim 74.1 \pm {}^{2.1}_{1.2}$ ka BP and the earlier feature at $\sim 82.0 \pm 1.0$ ka BP rather than 76.7 ± 1 and 84.3 ± 0.7 ka BP, respectively. At a $\delta^{234}U_i$ of 141‰, the apparent age of the MIS-5c deposit is around ~ 98 ka rather than 101 ka. The long residence time of uranium in the ocean precludes very large shifts in $\delta^{234}U$ [34]. However, small and/or local variations in $\delta^{234}U$ of less than 10‰ on short timescales cannot be ruled out. Further study of uranium balance in the oceans is required to test this hypothesis.

4. Sea level and climatic interpretations

The identification of two MIS-5a morphologically distinct coral-terrace deposits with distinct ages and large age separation (~ 7 ka) could either (i) represent two sea-level oscillations or (ii) be an artefact of a discrete tectonic uplift event. The currently exposed facies of the deposits do not allow us to clearly distinguish between these two alternatives. However, comparisons with other sea level and climate records, made in the following sections, supports the suggestion that MIS-5a was characterised by at least two rapid sea-level oscillations.

4.1. Sea level

Suborbital sea-level oscillations during MIS-5a are not consistent with a simple Milankovitch insolation-forcing model and imply that additional processes influence global ice volume at this time. An emerging picture of complex variability in sea level and climate during MIS-5 supports these observations. In particular, the morphology of multiple sub-terraces at Huon Peninsula, Papua New Guinea also indicates a complex structure during this period [6,9,35–38]. The Huon Peninsula coral terraces record more events in the sea level than seen at Barbados in this study. This is not unexpected because the higher uplift rates at Huon Peninsula result in the exposure of additional features. At least five distinct terraces at Huon (VIa, VIb, Va$_{outer}$, Va$_{main}$, Vb in the notation of [6]) represent oscillations during MIS-5a and 5c (Fig. 4b) although the ages of these reefs are not as well constrained as at Barbados. The above literature data links the reef Va$_{outer}$ with the classic MIS-5a high-stand at ∼ 84 ka (Fig. 4b). The poorly developed sub-reef Vb at Huon Peninsula appears to not be a constructional reef crest and has not been dated, but may be an erosional feature correlated with the 77-ka feature identified at Barbados in this study. The emerging picture of complex sea level changes at Barbados highlights the need for further systematic dating studies of the uplifted MIS-5 coral reef terraces at Huon Peninsula.

Most studies of MIS-5a deposits around the world yield ages corresponding to the older (∼ 84 ka) Barbados deposit identified in this study (a short review of MIS-5a deposits in the Caribbean and surrounding region can be found in [39]). However, there is a notable dearth of evidence for the ∼ 77-ka feature at other locations. This could be due to a number of reasons. Possibly the 77-ka oscillation was very rapid, or coincided with less favourable conditions for reef formation in most locations. It is also possible that the sea level at 77 ka was lower and did not overprint the earlier event at most Caribbean locations. On the US East coast, the ages of coastal deposits range between 72 and 84 ka BP, with younger deposits dominating at northernmost sites [40]. The overprinting of the older deposits with the younger event at these sites, in contrast to most Caribbean locations can be explained by the effects of glacio-hydro-isostasy, which predicts that the relative heights of the consecutive MIS-5a sea-level high-stands change as a function of distance from the great North American Ice Sheets [39].

4.2. Climate

The mechanisms that are involved in controlling climate and ice-sheet periodicity and how these vary in different mean climate states remain the focus of much climate research that is carried out today. In contrast to the orbital periodicity predicted by Milankovitch-forcing models, the discovery of decadal to millenial scale climate variations during MIS-3 recorded in the Greenland ice cores [41] drew attention to the need for alternative mechanisms to explain short period climate variability. Recently, it has been shown that for MIS-3 there is a direct correlation between Heinrich event discharges in the North Atlantic and sea-level rises recorded by terrace construction at Huon Peninsula [42,43]. Those observations emphasised the important link between rapid climate change and ice sheet instability during that time period.

The emerging picture of MIS-5 climate, including the results of the present study, extends the suborbital-period climatic behaviour from the heavily glaciated MIS-3 to the less glaciated MIS-5. A compilation of climate records for the MIS-5 interval also displays a shorter period variability that is strikingly similar to that suggested by the coral reef data. In particular, a sea-level record inferred from Red Sea $\delta^{18}O$ variability [44] shows large oscillations that correlate to the MIS-5a and MIS-4 excursions constrained in the present study and at Huon Peninsula [32] (see Fig. 4). Other climate records such as Greenland $\delta^{18}O$ [41], North Atlantic Ocean sea-surface temperature, and episodes of enhanced ice rafted debris (IRD) deposition in the North Atlantic [45,46] are also shown in Fig. 4. These records do not have independent age control, however the comparison suggests there is a rough correspondence of events recorded by the coral terrace data and those in the Greenland ice cores and in North Atlantic sediments. This implies that sea level during MIS-5a and 5c, as for MIS-3, is also related to northern hemisphere ice sheets dynamics and associated interruptions to oceanic circulation.

The older MIS-5a event identified in this study occurred at the time of the associated rise in 65°N summer insolation. Ice melt induced by Milankovitch-forcing may have been involved in triggering the initial destabilisation of shelf-based ice sheets but this does not provide an explanation for the additional oscillations observed in the sea-level and climate records. The events observed in the latter stages of
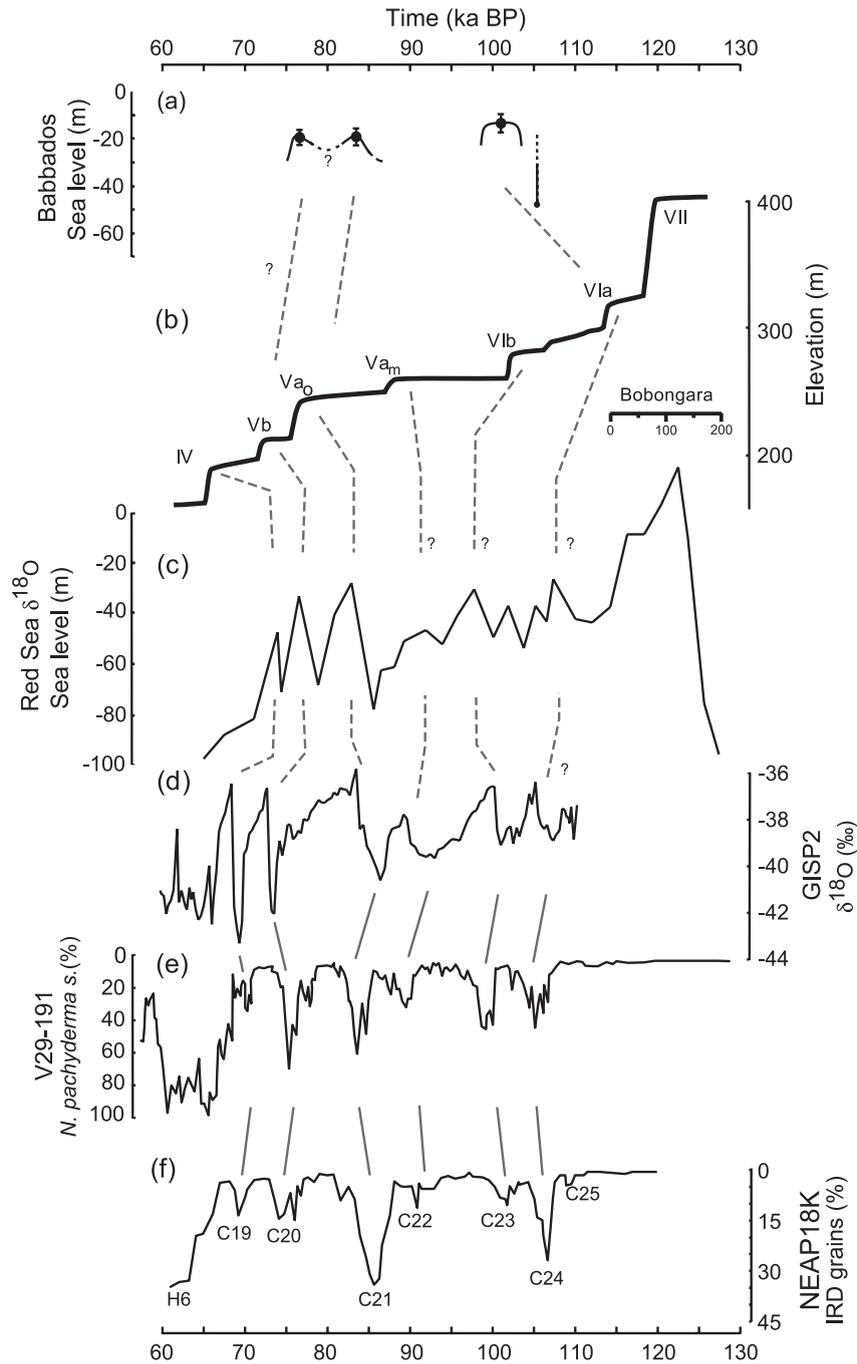
MIS-5 North Atlantic records display similar characteristics to that of the millennial scale Heinrich events observed during MIS-3 [47], but there are also some significant differences. The magnitudes of the MIS-5 ice-rafting (IRD) events recorded in the North Atlantic are much smaller that that of Heinrich events. Furthermore, the composition of MIS-3 Heinrich layers indicate that this material was from massive collapse of the Laurentide Ice Sheet, whereas the composition of the MIS-5 layers indicates multiple source regions [45]. These differences imply that although there was sufficient ice during the latter part of MIS-5 to be susceptible to collapse, the distribution or source of rafted ice during MIS-3 and MIS-5 was different. In general MIS-5 ice volumes were smaller and the Laurentide ice sheet may have been less susceptible to destabilisation and large-scale collapse at this time, with little or no ice over Hudson Bay, than at later times [48]. After the last interglacial period, the European ice sheet was initiated over the Arctic continental shelf region and advanced southward onto the Eurasian continent later during MIS-5 [49]. This may have provided an alternative source of ice, which, being shelf-based, was susceptible to rapid destabilisation and collapse, thereby triggering the climatic interruptions observed in this region [50]. The similar periodicity (~ 7 ka) of the events during MIS-3 and MIS-5 suggests that another pacemaker may be responsible, perhaps involving ocean circulation dynamics. Irrespective of the mechanism, these comparisons demonstrate that the complex linkages between ice volume and climate instabilities existed throughout the last glacial cycle and were not restricted to heavily glaciated periods such as MIS-3.

5. Conclusions

We have used high-precision U–Th TIMS analysis techniques to precisely constrain the timing of MIS-5a

Fig. 4. Comparison of MIS-5a and 5c sea level oscillations constrained in this study with other sea level and climate records for the same period. (a) MIS-5a and 5c Barbados sea level oscillations. The calculation of relative sea level at Barbados is based on the assumption of constant uplift since the last interglacial period. Where applicable, corresponding deposits on the south and west coasts (judged by overlap in the age-δ^{234}U data) are assigned the same mean age, which is then assigned to the elevation of the crest of the reef deposit (with an allowance for a crest growth depth of 1 ± 1 m). The rate of uplift inferred for each transect is calculated based on the elevation of the last interglacial reef crest [20], an age of 128 ± 3 ka, and a paleo-sea level of 4 ± 2 m [28,52]. For the south coast section, this gives an uplift rate of 0.27 ± 0.03 m/ka and for the west coast 0.45 ± 0.03 m/ka. Where applicable, the sea levels for corresponding features at the two transects are then averaged. The calculated sea level for the 77 ka feature identified on the south coast (site IM) is therefore $- 18 \pm 4$ m, and the 84-ka feature, represented by deposits (PEP and BRB3) occurred at a sea level of $- 19 \pm 4$ m. Combining estimates of relative sea level from different localities to produce a composite sea level curve, e.g. [17], is not valid unless the effects of glacio-hydro-isostasy are taken into account [39]. For example, the relative sea level predicted for the MIS-5a event is more than 10 m higher at Florida than at Barbados due to the glacio-isostatic effects of the Laurentide ice sheet. The MIS-5c high sea level at 101 ka, represented by sites U18, U15 and BRB4, was at $- 14 \pm 4$ m. Site BRB1 represents coral growth early during MIS-5c, but because it is indicative of deeper water growth (lower than $- 15$ m) it does not give a precise constraint on sea level. (b) Schematic cross-section of MIS-5 reefs at Bobongara, Huon Peninsula, Papua New Guinea (from a 2001 expedition with John Chappell, TME, EKP and Eugene Wallensky) to illustrate the complexity of reef development at that location. Reefs VIa and VIb are thought to correspond to sub-stage 5c [6,9,35] and Reef Va-outer represents coral growth during the 'classic' sub-stage 5a highstand at around 84 ka [37]. Sub-reef Va$_{main}$ is only visible at locations of highest uplift and is thought to represent an early sea level rise prior to the peak of MIS-5a at 84 ka [38], an interpretation that is supported by evidence of relatively high sea level at Florida by 93 ka BP [11]. The poorly developed and un-dated sub-reef Vb appears to not be a constructional reef crest but may be correlated with the 77-ka feature identified at Barbados in this study. Dating of reef IV corals gives a mean age of ~ 71 ka and appears to represent a sea level oscillation during the transition from MIS-5 to 4 [32]. The dating control on the Huon Peninsula reefs is not as clear as it is at Barbados but possible correspondence with the Barbados features are suggested. (c) Low-resolution sea level curve calculated from a Red Sea δ^{18}O record with suggested correlations to Huon Peninsula and Barbados coral reef features [44]. Three large, rapid sea level oscillations during MIS-5a and the MIS-5a to 4 transition in the Red Sea records correlate well with the three sea level highstands constrained for that period in this study at Barbados and at Huon Peninsula [32]. The oscillations in this record during MIS-5c are broader and less distinct, which may be consistent with the broader MIS-5c feature identified in this study (Fig. 2). (d) GISP2 δ^{18}O record [41] plotted on ice core timescale displays rapid oscillations in climate in that region with a similar frequency to that of a composite sea level record from Barbados and Huon Peninsula. (e) V29-191 N. pachyderma (s.) abundance-high values indicate low SST [46]. Time scales of V29-191 records are approximate, but can be directly correlated with the NEAP18K SST record (not shown here) and episodes of enhanced IRD deposition (bottom panel). (f) NEAP18K IRD record showing episodes of enhanced IRD deposition, with time-scale tied to GISP2 δ^{18}O using sediment core lightness [45]. Possible links between sea-level records and climate oscillations are indicated. Periods of sea-level rise may be correlated with ice sheet collapse, IRD deposition and cold episodes in the North Atlantic.

and 5c coral deposits at Barbados. The timing of three sea-level events during MIS-5a and 5c, each associated with a distinct morphological reef terrace unit at Barbados, have been determined. The mean age of these deposits, assuming oceanic δ^{234}U at the time of deposition was equal to the present day, are centred at 76.7 ± 1.0, 84.3 ± 0.7 and $\sim 101 \pm 3$ ka. This data set more than doubles the existing number of high precision U-series ages for the MIS-5a and 5c Barbados terraces. The present study demonstrates the effectiveness of high-precision U-series dating, when combined with extensive sampling and detailed stratigraphic mapping [20], to distinguishing between closely spaced events in the sea-level coral record.

The Barbados deposits with ages of ~ 101 and ~ 84 ka define the timing of the classic MIS-5a and 5c events, while the youngest at ~ 77 ka may represent an additional sea-level highstand during late MIS-5a. These results, combined with the observation of multiple MIS-5a and 5c sub-terraces at Huon Peninsula demonstrate that Milankovitch orbital forcing alone cannot account for the observed changes in global ice volume. The existence of suborbital-period sea-level oscillations during MIS-5 is also supported by the presence of correlated climate interruptions in the North Atlantic. A comparison of these records with the sea-level data shows that complex feedbacks between ice sheets and regional climate, which are characteristic of the glacial conditions in MIS-3, were also active during the relatively warm period following the last interglacial.

Acknowledgements

References

[1] M. Milankovitch, Kanon der Erdbestrahlung (Canon of insolation and the ice age problem), Sect. Math. Nat. Sci. 33 (1941) 132 (English translation by Israel Program for Scientific Translations, Jerusalem, 1969).

[2] J.D. Hays, J. Imbrie, N.J. Shackleton, Variations in the earth's orbit: pacemaker of the ice ages, Science 194 (1976) 1121–1132.

[3] A.H.L. Voelker, Global distribution of centennial-scale records for marine isotope stage (MIS) 3: a database, Quat. Sci. Rev. 21 (2002) 1185–1212.

[4] H.H. Veeh, J. Chappell, Astronomical theory of climatic change: support from New Guinea, Science 167 (1970) 862–865.

[5] K.J. Mesolella, R.K. Matthews, W.S. Broecker, D. Thurber, The astronomical theory of climatic change: Barbados data, J. Geol. 77 (1969) 250–274.

[6] J. Chappell, Geology of coral terraces, Huon Peninsula, New Guinea: a study of quaternary tectonic movements and sea-level changes, Geol. Soc. Amer. Bull. 85 (1974) 553–570.

[7] M.L. Bender, R.G. Fairbanks, F.W. Taylor, R.K. Matthews, J.G. Goddard, W.S. Broecker, Uranium-series dating of the Pleistocene reef tracts of Barbados, West Indies, Geol. Soc. Amer. Bull. 90 (1979) 577–594.

[8] G. Schellmann, U. Radtke, A revised morpho- and chronostratigraphy of the Late and Middle Pleistocene coral reef terraces on Southern Barbados (West Indies), Earth-Sci. Rev. 64 (2004) 157–187.

[9] T.M. Esat, M.T. McCulloch, J. Chappell, B. Pillans, A. Omura, Rapid fluctuations in sea level recorded at Huon Peninsula during the penultimate deglaciation, Science 283 (1999) 197–201.

[10] K.R. Ludwig, D.R. Muhs, K.R. Simmons, R.B. Halley, E.A. Shinn, Sea-level records at ~80ka from tectonically stable platforms: Florida and Bermuda, Geology 24 (1996) 211–214.

[11] M.A. Toscano, J. Lundberg, Submerged Late Pleistocene reefs on tectonically stable S.E. Florida margin: High precision geochronology, stratigraphy, resolution of Substage 5a sea-level elevation, and orbital forcing, Quat. Sci. Rev. 18 (1999) 753–767.

[12] D.R. Muhs, K.R. Simmons, B. Steinke, Timing and warmth of the Last Interglacial period: new U-series evidence from Hawaii and Bermuda and a new fossil compilation for North America, Quat. Sci. Rev. 21 (2002) 1355–1383.

[13] E. Bard, B. Hamelin, R.G. Fairbanks, U–Th ages obtained by mass spectrometry in corals from Barbados: sea level during the past 130,000 years, Nature 346 (1990) 456–458.

[14] R.L. Edwards, H. Cheng, M.T. Murrell, S.J. Goldstein, Protactinium-231 dating of carbonates by thermal ionization mass spectrometry: implication for quaternary climate change, Science 276 (1997) 782–786.

[15] C.D. Gallup, R.L. Edwards, R.G. Johnson, The timing of high sea levels over the past 200,000 years, Science 263 (1994) 796–800.

[16] R.L. Edwards, J.H. Chen, T.L. Ku, G.J. Wasserburg, Precise timing of the last interglacial period from mass spectrometric determination of thorium-230 in corals, Science 236 (1987) 1547–1553.

[17] K.B. Cutler, R.L. Edwards, F.W. Taylor, H. Cheng, J.F.

Adkins, C.D. Gallup, P.M. Cutler, G.S. Burr, A.L. Bloom, Rapid sea level fall and deep-ocean temperature change since the last interglacial period, Earth Planet. Sci. Lett. 206 (2003) 253–271.

[18] G. Schellmann, U. Radtke, in: Neue Ergebnisse zur Verbreitung und Altersstellung gehobener Korallenriffterrassen im Süden von Barbados, vol. 20, Bamberger Geographische Schriften, Bamberg, 2001, pp. 201–244.

[19] G. Schellmann, U. Radtke, The coral reef terraces of Barbados—a guide, Barbados 2002—International Conference on "Quaternary Sea Level Change" with Field Trips and 4th Annual Meeting of IGCP Project 437 "Coastal Environmental Change during sea level highstands: A global synthesis with implications for management of future coastal change". INQUA Commission on Coastlines, IGU Commission on Coastal Systems, University of Bamberg, Bamberg, 2002. 118 pp.

[20] G. Schellmann, U. Radtke, The marine Quaternary of Barbados, Koelner Geogr. Arb. 81 (in press).

[21] G. Schellmann, U. Radtke, E.-K. Potter, T.M. Esat, M.T. McCulloch, Comparison of ESR and TIMS U/Th dating of marine isotope stage (MIS) 5e, 5c, and 5a coral from Barbados—implications for palaeo sea-level changes in the Caribbean, Quat. Int. (2004) (in press).

[22] K.J. Mesolella, Zonation of the uplifted Pleistocene coral reefs on Barbados, West Indies, Science 196 (1967) 638–640.

[23] C.H. Stirling, T.M. Esat, M.T. McCulloch, K. Lambeck, High-precision U-series dating of corals from Western Australia and implications for the timing and duration of the Last Interglacial, Earth Planet. Sci. Lett. 135 (1995) 115–130.

[24] H. Cheng, R.L. Edwards, M.T. Murrell, T.M. Benjamin, Uranium–thorium–protactinium dating systematics, Geochim. Cosmochim. Acta 62 (1998) 3437–3452.

[25] W.G. Thompson, M.W. Spiegelman, S.L. Goldstein, R.C. Speed, An open-system model for U-series age determinations of fossil corals, Earth Planet. Sci. Lett. 210 (2003) 365–381.

[26] B. Villemant, N. Feuillet, Dating open systems by the U-238–U-234–Th-230 method: application to Quaternary reef terraces, Earth Planet. Sci. Lett. 210 (2003) 105–118.

[27] D. Scholz, A. Mangini, T. Felis, U-series dating of diagenetically altered fossil reef corals, Earth Planet. Sci. Lett. 218 (2004) 163–178.

[28] C.H. Stirling, T.M. Esat, K. Lambeck, M.T. McCulloch, Timing and duration of the last interglacial: evidence for a restricted interval of widespread coral reef growth, Earth Planet. Sci. Lett. 160 (1998) 745–762.

[29] D. Delanghe, E. Bard, B. Hamelin, New TIMS constraints on the uranium-238 and uranium-234 in seawaters from the main ocean basins and the Mediterranean Sea, Mar. Chem. 80 (2002) 79–93.

[30] L.F. Robinson, N.S. Belshaw, G.M. Henderson, U and Th isotopes in seawater and modern carbonates from the Bahamas, Geochim. Cosmochim. Acta 68 (2004) 1777–1789.

[31] B. Hamelin, E. Bard, A. Zindler, R.G. Fairbanks, U-234/U-238 mass spectrometry of corals: how accurate is the U–Th age of the last interglacial period? Earth Planet. Sci. Lett. 106 (1991) 169–180.

[32] J. Chappell, A. Omura, T.M. Esat, M. McCulloch, J. Pandolfi, Y. Ota, B. Pillans, Reconciliation of late Quaternary sea levels derived from coral terraces at Huon Peninsula with deep sea oxygen isotope records, Earth Planet. Sci. Lett. 141 (1996) 227–236.

[33] Y. Yokoyama, Sea-Level Change in Australasia and the Radiocarbon Time Scale During the Last 50,000 Years, Australian National University, Canberra, 1999.

[34] G.M. Henderson, Seawater (U-234/U-238) during the last 800 thousand years, Earth Planet. Sci. Lett. 199 (2002) 97–110.

[35] J. Chappell, N.J. Shackleton, Oxygen isotopes and sea level, Nature 324 (1986) 137–140.

[36] K. Lambeck, J. Chappell, Sea level change through the last glacial cycle, Science 292 (2001) 679–686.

[37] A.L. Bloom, W.S. Broecker, J.M.A. Chappell, R.K. Matthews, K.J. Mesolella, Quaternary sea level fluctuations on a tectonic coast: new Th-230/U-234 dates from the Huon Peninsula, New Guinea, Quat. Res. 4 (1974) 185–205.

[38] A. Omura, J. Chappell, A.L. Bloom, M.T. McCulloch, T.M. Esat, K. Sasaki, Y. Kawada, Alpha-spectrometric ^{230}Th/^{234}U dating of Pleistocene corals, in: Y. Ota (Ed.), Study on Coral Reef Terraces of the Huon Peninsula, Papua New Guinea. IGCP 274, Yokohama, 1994.

[39] E.K. Potter, K. Lambeck, Reconciliation of sea-level observations in the Western North Atlantic during the last glacial cycle, Earth Planet. Sci. Lett. 217 (2004) 171–181.

[40] J.F. Wehmiller, K.R. Simmons, H. Cheng, R.L. Edwards, J. Martin-McNaughton, L.L. York, D.E. Krantz, C.C. Shen, Uranium-series coral age from the US Atlantic Coastal Plain—the "80 ka problem" problem revisited, Quat. Int. (2004) (in press).

[41] P.M. Grootes, M. Stuiver, Oxygen 18/16 variability in Greenland snow and ice with 10(−3)- to 10(5)-year time resolution, J. Geophys. Res.-Oceans 102 (1997) 26455–26470.

[42] Y. Yokoyama, T.M. Esat, K. Lambeck, Coupled climate and sea-level changes deduced from Huon Peninsula coral terraces of the last ice age, Earth Planet. Sci. Lett. 193 (2001) 579–587.

[43] J. Chappell, Sea level changes forced ice breakouts in the last glacial cycle: new results from coral terraces, Quat. Sci. Rev. 21 (2002) 1229–1240.

[44] M. Siddall, E.J. Rohling, A. Almogi-Labin, C. Hemleben, D. Meischner, I. Schmelzer, D.A. Smeed, Sea-level fluctuations during the last glacial cycle, Nature 423 (2003) 853–858.

[45] M.R. Chapman, N.J. Shackleton, Global ice-volume fluctuations, North Atlantic ice-rafting events, and deep-ocean circulation changes between 130 and 70 ka, Geology 27 (1999) 795–798.

[46] J.F. McManus, G.C. Bond, W.S. Broecker, S. Johnsen, L. Labeyrie, S. Higgins, High-resolution climate records from the North-Atlantic during the last interglacial, Nature 371 (1994) 326–329.

[47] G. Bond, W.S. Broecker, S. Johnsen, J. McManus, L. Labeyrie, J. Jouzel, G. Bonani, Correlations between climate records from North Atlantic sediments and Greenland ice, Nature 365 (1993) 143–147.

[48] J. Kleman, J. Fastook, A.P. Stroeven, Geologically and geomorphologically constrained numerical model of Laurentide Ice Sheet inception and build-up, Quat. Int. 95-6 (2002) 87–98.

[49] J.I. Svendsen, V.I. Astakhov, D.Y. Bolshiyanov, I. Demidov, J.A. Dowdeswell, V. Gataullin, C. Hjort, H.W. Hubberten, E. Larsen, J. Mangerud, M. Melles, P. Möller, M. Saarnisto, M.J. Siegert, Maximum extent of the Eurasian ice sheets in the Barents and Kara Sea region during the Weichselian, Boreas 28 (1999) 234–242.

[50] K. Lambeck, T.M. Esat, E.K. Potter, Links between climate and sea levels for the past three million years, Nature 419 (2002) 199–206.

[51] A.L. Berger, M.-F. Loutre, Insolation values for the climate of the last 10 million years, Quat. Sci. Rev. 10 (1991) 297–317.

[52] J.H. Chen, H.A. Curran, B. White, G.J. Wasserburg, Precise chronology of the last interglacial period: U-234–Th-230 data from fossil coral reefs in the Bahamas, Geol. Soc. Amer. Bull. 103 (1991) 82–97.

[53] W.S. Broecker, A preliminary evaluation of uranium series inequilibrium as a tool for absolute age measurement on marine carbonates, J. Geophys. Res. 68 (1963) 2817–2834.

[54] J.W. Meadows, R.J. Armani, E.L. Callis, A.M. Essling, Half-life of Th-230, Phys. Rev., C 22 (1980) 750–754.

[55] P. De Bievre, K.F. Lauer, Y. LeDuigon, H. Moret, G. Muschenborn, J. Spaepen, A. Spernol, R. Vaninbroukx, V. Verdingh, The half-life of 234-U, in: M.L. Hurrell (Ed.), Proc. Int. Conf. Chem. Nucl. Data, Measurements and Applications, Canterbury, Institute of Civil Engineers, London, 1971, pp. 221–225.

[56] M. Lounsbury, R.W. Durham, The alpha-half-life of U-234, in: M.L. Hurrell (Ed.), Proc. Int. Conf. Chem. Nucl. Data, Measurements and Applications, Canterbury, Institute of Civil Engineers, London, 1971, pp. 215–219.

[57] R.L. Edwards, J.H. Chen, G.J. Wasserburg, 238U–234U–230Th–232Th systematics and the precise measurement of time over the past 500,000 years, Earth Planet. Sci. Lett. 81 (1987) 175–192.

[58] T.M. Esat, Charge collection thermal ion mass spectrometry of thorium, Int. J. Mass Spectrom. Ion Process. 148 (1995) 159–170.

[59] K.R. Ludwig, K.R. Simmons, B.J. Szabo, I.J. Winograd, J.M. Landwehr, A.C. Riggs, R.J. Hoffman, Mass-spectrometric Th-230–U-234–U-238 dating of the devils-hole calcite vein, Science 258 (1992) 284–287.